Bottom quark dynamics from nonprompt D^0 and J/ψ production in Pb+Pb collisions at $\sqrt{s_{NN}} = 5.02$ TeV

Wen-Jing Xing,[1] Shu-Qing Li,[2,*] Shanshan Cao,[1,†] and Guang-You Qin[3,‡]

[1]*Institute of Frontier and Interdisciplinary Science, Shandong University, Qingdao, Shandong 266237, China*

[2]*School of Physics and Electronic Engineering, Jining University, Qufu, Shandong 273155, China*

[3]*Institute of Particle Physics and Key Laboratory of Quark and Lepton Physics (MOE), Central China Normal University, Wuhan, Hubei 430079, China*

(Received 28 April 2024; accepted 24 July 2024; published 12 August 2024)

We study bottom quark energy loss via the nuclear modification factor (R_{AA}) and elliptic flow (v_2) of nonprompt D^0 and J/ψ in relativistic heavy-ion collisions at the Large Hadron Collider (LHC). The space-time profile of quark-gluon plasma is obtained from the CLVISC hydrodynamics simulation, the dynamical evolution of heavy quarks inside the color deconfined QCD medium is simulated using a linear Boltzmann transport model that combines Yukawa and string potentials of heavy-quark-medium interactions, the hadronization of heavy quarks is performed using a hybrid coalescence-fragmentation model, and the decay of B mesons is simulated via PYTHIA. Using this numerical framework, we calculate the transverse momentum (p_T) dependent R_{AA} and v_2 of direct D mesons, B mesons, and nonprompt D^0 and J/ψ from B meson decay in Pb+Pb collisions at $\sqrt{s_{NN}} = 5.02$ TeV. We find the mass hierarchy of the nuclear modification of prompt D and B mesons depends on their p_T. Both R_{AA} and v_2 of heavy flavor particles show strong p_T and centrality dependences due to the interplay between parton energy loss, medium geometry and flow, and hadronization of heavy quarks. Nonprompt D^0 and J/ψ share similar patterns of R_{AA} and v_2 to B mesons except for a p_T shift during the decay processes. Therefore, future more precise measurements on nonprompt D^0 and J/ψ can help further pin down the bottom quark dynamics inside the quark-gluon plasma.

DOI: 10.1103/PhysRevC.110.024903

I. INTRODUCTION

The quark-gluon plasma (QGP), which consists of deconfined quarks and gluons as predicted by quantum chromodynamics (QCD) on the lattice, has been created in relativistic heavy-ion collisions performed at the Relativistic Heavy-Ion Collider (RHIC) and the Large Hadron Collider (LHC) [1,2]. Extensive studies have shown that the hot and dense QGP produced in these energetic nuclear collisions has two remarkable properties: small shear viscosity to entropy density ratio (or specific viscosity) [3–7], and high opacity to the propagation of high-energy jet partons [8–14].

Heavy quarks (charm and bottom quarks) are important hard probes of the QGP [15–17]. They are mostly produced from the hard scatterings in the early stage of heavy-ion collisions, and then probe the entire history of the expanding QGP. During their propagation through the QGP, heavy quarks interact with the medium and lose energy via collisional and radiative processes [18–21]. The energy loss of heavy quarks in the QGP can be quantified by the nuclear modification factor R_{AA}, defined as the ratio of the particle yield in a given centrality class in nucleus-nucleus (AA) collisions (dN_{AA}/dp_T), scaled by the average number of binary nucleon-nucleon collisions ($N_{\rm coll}$), to the particle yield in proton-proton (pp) collisions (dN_{pp}/dp_T). Experimental measurements have shown that the R_{AA} of heavy flavor particles produced in Au+Au collisions at RHIC and Pb+Pb collisions at the LHC is significantly below unity at high p_T [22–24], indicating substantial energy loss of heavy quarks inside the QGP medium due to their interactions with the medium constituents [25–49].

Another important observable to probe the geometrical and dynamical properties of the QGP is the azimuthal anisotropy of the momentum space distribution of final state (soft and hard) hadrons [50–54], which can be quantified by the Fourier coefficients of the particle distribution $dN/d\phi$ in the azimuthal plane. These anisotropy coefficients can be calculated as $v_n = \langle \cos[n(\phi - \Phi_n)] \rangle$, with Φ_n being the nth-order event plane angle. For example, v_2 is called elliptic flow, which mainly originates from the elliptic shape of the produced QGP matter. Quantum fluctuations of the initial state (or colliding nuclei) can also contribute to the anisotropic flow, especially for odd flow harmonics and in ultra-central

*Contact author: lisq79@jnxy.edu.cn

†Contact author: shanshan.cao@sdu.edu.cn

‡Contact author: guangyou.qin@ccnu.edu.cn

collisions [55,56]. As for heavy quarks, due to their interactions with the anisotropic QGP, the final momentum distributions of heavy quarks and their daughter hadrons are also anisotropic. At high $p_{\rm T}$, the heavy flavor hadron v_2 is sensitive to the energy loss difference of heavy quarks along different paths through the QGP. At low and intermediate $p_{\rm T}$, their v_2 is sensitive to the collective flow of the QGP medium, since low $p_{\rm T}$ heavy quarks can pick up the QGP flow either by direct interactions with the medium through diffusive process or by coalescence with thermal light partons inside the medium during hadron formation [57–64]. Experimental data have shown that D mesons have positive v_2 at RHIC and the LHC [65–68], indicating that charm quarks can build up significant collective flow through scatterings with an anisotropic QGP medium as well as the hadronization process. The magnitude of the D meson v_2 is similar to the light flavor hadron v_2 at intermediate $p_{\rm T}$, indicating that the relaxation time of low $p_{\rm T}$ charm quarks might be comparable to or even shorter than the lifetime of the QGP.

In this work, we focus on bottom quark evolution in relativistic heavy-ion collisions. Due to their even larger mass than charm quarks, bottom quarks provide a unique probe of the QGP properties. First, they suffer much smaller cold nuclear matter effect than charm quarks [69], thus offer clean observables to study the hot nuclear matter effect. In addition, bottom quarks provide a better tool to study the "dead cone" effect which strongly depends on the mass-to-energy ratio (m_Q/E) of heavy quarks [70–74]. Therefore, at low to intermediate $p_{\rm T}$, bottom quarks are expected to experience less diffusion than charm quarks, and thus are harder to reach thermalization with QGP medium [49,57,59]. Recently, ALICE, ATLAS, and CMS Collaborations have measured the R_{AA} and v_2 of nonprompt D^0 and J/ψ decayed from bottom hadrons [75–84]. Considering the large uncertainties of the current data directly on B mesons, these measurements on nonprompt D^0 and J/ψ provide an important supplementary opportunity for studying bottom quark interaction with the QGP in relativistic heavy-ion collisions. We will report our study on the R_{AA} and v_2 of bottom decayed D^0 and J/ψ, and compare them to results of prompt D mesons directly produced from charm quark hadronization, in Pb+Pb collisions at $\sqrt{s_{NN}} = 5.02$ TeV from low to high $p_{\rm T}$ regimes. The rest of this paper will be organized as follows. In Sec. II, we will present our theoretical framework to study heavy quark evolution in relativistic heavy-ion collisions. The numerical results for prompt D mesons, B mesons, and nonprompt D^0 and J/ψ from B meson decay will be presented and compared to available data at the LHC in Sec. III. Section IV will contain our summary.

II. THEORETICAL FRAMEWORK: LBT-PNP MODEL

In this work, we use our linear Boltzmann transport model that combines perturbative and nonperturbative interactions (LBT-PNP) [59] to simulate heavy quark scatterings through a color-deconfined medium. In the LBT model [19,85,86], one solves the following Boltzmann equation for the evolution of the phase space distribution of heavy quarks (denoted by "a") inside the QGP using the Monte Carlo method:

$$P_a \cdot \partial f_a(x,p) = E_a(\mathcal{C}_{\rm el} + \mathcal{C}_{\rm inel}). \tag{1}$$

The right-hand side includes the contributions from both elastic and inelastic scatterings between heavy quarks and constituent partons of the medium, as denoted by the collision integrals $\mathcal{C}_{\rm el}$ and $\mathcal{C}_{\rm inel}$, respectively.

To simulate elastic scatterings between heavy quarks and medium partons, one calculates the scattering rates $\Gamma_{ab\to cd}$ for a binary collision process $a+b\to c+d$ using the following formula:

$$\begin{aligned}\Gamma_{ab\to cd}(\vec{p}_a,T) = \frac{\gamma_b}{2E_a}\int \frac{d^3p_b}{(2\pi)^3 2E_b}\frac{d^3p_c}{(2\pi)^3 2E_c}\frac{d^3p_d}{(2\pi)^3 2E_d} \\ \times f_b(\vec{p}_b,T)[1\pm f_c(\vec{p}_c,T)][1\pm f_d(\vec{p}_d,T)] \\ \times \theta(s-(m_a+\mu_d)^2)(2\pi)^4 \\ \times \delta^{(4)}(p_a+p_b-p_c-p_d)|\mathcal{M}_{ab\to cd}|^2.\end{aligned} \tag{2}$$

In the above equation, γ_b is the degeneracy factor of parton b, f_b and f_d are thermal distributions of the medium partons, $1\pm f$ is the Bose enhancement or Fermi suppression factor for the final states (neglected for heavy quark c due to their dilute distribution in this work), and the θ function accounts for the thermal mass effect on medium partons, where μ_d represents the Debye mass. In this calculation, the masses of charm and bottom quarks are taken as $M_c = 1.27$ GeV and $M_b = 4.19$ GeV, and the medium partons are taken to be massless. The key information about the microscopic elastic scattering process is contained in the matrix element $\mathcal{M}_{ab\to cd}$.

In the LBT-PNP model [59], the matrix element $\mathcal{M}_{ab\to cd}$ for elastic scatterings includes both perturbative and nonperturbative interactions between heavy quarks and medium constituents. More specifically, we use the following parametrized Cornell-type potential for the interaction between a heavy quark and a medium parton,

$$V(r) = V_{\rm Y}(r) + V_{\rm S}(r) = -\frac{4}{3}\alpha_{\rm s}\frac{e^{-m_d r}}{r} - \frac{\sigma e^{-m_s r}}{m_s}. \tag{3}$$

One can see that the above potential includes both short-range Yukawa interaction and long-range color confining interaction, the later of which is also called the string term. In these two terms, $\alpha_{\rm s}$ and σ are the coupling strengths for the Yukawa and string interactions respectively, m_d and m_s are their corresponding screening masses, which are taken to be temperature dependent as $m_d = a + bT$ and $m_s = \sqrt{a_s + b_s T}$. In the LBT-PNP model [59], the values and functional forms of the model parameters are fitted from the suppression and flow data of D mesons at RHIC and the LHC as: $\alpha_{\rm s} = 0.27$, $\sigma = 0.45$ GeV^2, $m_d = 2T + 0.2$ GeV, and $m_s = \sqrt{0.1\ {\rm GeV}\times T}$. The potential evaluated using these parameters reasonably agrees with the lattice data.

To calculate the matrix element $\mathcal{M}_{ab\to cd}$, one takes the Fourier transformation and obtains the above Cornell-type potential in the momentum space as

$$V(\vec{q}) = -\frac{4\pi\alpha_{\rm s}C_F}{m_d^2+|\vec{q}|^2} - \frac{8\pi\sigma}{\left(m_s^2+|\vec{q}|^2\right)^2}, \tag{4}$$

with $\vec{q}$ being the momentum exchange between heavy quarks and medium constituents. To calculate the matrix element for two-body processes: $Qq \to Qq$ and $Qg \to Qg$, in which gluons with momentum $\vec{q}$ are exchanged, we treat the above in-medium Cornell-type potential as the effective gluon propagator (field). Assuming a scalar interaction vertex for the string term, the scattering amplitude can be written as

$$i\mathcal{M} = \mathcal{M}_{\rm Y} + \mathcal{M}_{\rm S} = \bar{u}(p')\gamma^{\mu}u(p)V_{\rm Y}(\vec{q})\bar{u}(k')\gamma^{\nu}u(k) + \bar{u}(p')u(p)V_{\rm S}(\vec{q})\bar{u}(k')u(k). \quad (5)$$

Here, $\mathcal{M}_{\rm Y}$ and $\mathcal{M}_{\rm S}$ represent the matrix elements for the Yukawa and string terms respectively. Note that we still use a vector interaction vertex for the Yukawa term, which can reproduce the leading-order perturbative QCD result [87]. Since the in-medium potential represents the effective gluon propagator, the string term is only included for the t-channel scattering, i.e., by setting $|\vec{q}|^2 = -t$ in the above potential. Note that the color information of interaction vertices has been included in the interaction potential. For the $Qq \to Qq$ scattering process, the final amplitude squared is given by

$$|\mathcal{M}_{Qq}|^2 = \frac{64\pi^2\alpha_{\rm s}^2}{9}\frac{\left(s-m_Q^2\right)^2+\left(m_Q^2-u\right)^2+2m_Q^2t}{\left(t-m_d^2\right)^2} + \frac{(8\pi\sigma)^2}{N_c^2-1}\frac{t^2-4m_Q^2t}{\left(t-m_s^2\right)^4}; \quad (6)$$

and for the $Qg \to Qg$ process we have

$$|\mathcal{M}_{Qg}|^2 = \frac{64\pi^2\alpha_{\rm s}^2}{9}\frac{\left(s-m_Q^2\right)\left(m_Q^2-u\right)+2m_Q^2\left(s+m_Q^2\right)}{\left(s-m_Q^2\right)^2} + \frac{64\pi^2\alpha_{\rm s}^2}{9}\frac{\left(s-m_Q^2\right)\left(m_Q^2-u\right)+2m_Q^2\left(u+m_Q^2\right)}{\left(u-m_Q^2\right)^2} + 8\pi^2\alpha_{\rm s}^2\frac{5m_Q^4+3m_Q^2t-10m_Q^2u+4t^2+5tu+5u^2}{\left(t-m_d^2\right)^2} + 8\pi^2\alpha_{\rm s}^2\frac{\left(m_Q^2-s\right)\left(m_Q^2-u\right)}{\left(t-m_d^2\right)^2} + 16\pi^2\alpha_{\rm s}^2\frac{3m_Q^4-3m_Q^2s-m_Q^2u+s^2}{\left(s-m_Q^2\right)\left(t-m_d^2\right)} + \frac{16\pi^2\alpha_{\rm s}^2}{9}\frac{m_Q^2\left(4m_Q^2-t\right)}{\left(s-m_Q^2\right)\left(m_Q^2-u\right)} + 16\pi^2\alpha_{\rm s}^2\frac{3m_Q^4-m_Q^2s-3m_Q^2u+u^2}{\left(t-m_d^2\right)\left(u-m_Q^2\right)} + \frac{C_A}{C_F}\frac{(8\pi\sigma)^2}{N_c^2-1}\frac{t^2-4m_Q^2t}{\left(t-m_s^2\right)^4}, \quad (7)$$

with s, t, u being the Mandelstam variables. To obtain the Yukawa parts $|\mathcal{M}_{\rm Y}|^2$ in the above two expressions, we calculate $|\mathcal{M}_s|^2$, $|\mathcal{M}_u|^2$, $|\mathcal{M}_t|^2$, and their interference terms $|\mathcal{M}_s\mathcal{M}_t^*|$, $|\mathcal{M}_s\mathcal{M}_u^*|$, and $|\mathcal{M}_u\mathcal{M}_t^*|$ separately, and then replace t by $t-m_d^2$ in the denominators. Note that the form of the $|\mathcal{M}_{\rm Y}|^2$ part in Eq. (7) appears a little different from the form given by Ref. [87]. This is because the amplitude squared for the $Qg \to Qg$ scattering process is simplified in Ref. [87] by extracting a term $-16\pi^2\alpha_{\rm s}^2(2m_Q^2+t)/t$ from both $|\mathcal{M}_s\mathcal{M}_t^*|$ and $|\mathcal{M}_u\mathcal{M}_t^*|$, and then combine them with $|\mathcal{M}_t|^2$ to obtain $32\pi^2\alpha_{\rm s}^2(s-m_Q^2)(m_Q^2-u)/t^2$. If one introduces the Debye screening mass, i.e, replace t by $t-m_d^2$ in the denominators, based on the form in Ref. [87], as shown in Refs. [88–90], the matrix element would appear different from our Yukawa part in Eq. (7). However, they are the same when m_d is set as zero.

By summing over all possible scattering channels, one can obtain the total elastic scattering rate for a heavy quark propagating through the QGP according to Eq. (2). For a given time step $\Delta\tilde{t}$, the probability for a heavy quark to experience elastic scatterings with the QGP constituents can be calculated as $P_{\rm el}^a = 1 - e^{-\Gamma_{\rm el}^a\Delta\tilde{t}}$.

For inelastic scatterings between heavy quarks and the QGP, the scattering rate at a given time $\tilde{t}$ can be obtained as follows:

$$\Gamma_{\rm inel}^a(E_a, T, \tilde{t}) = \int dx\, dl_\perp^2 \frac{dN_g^a}{dx\, dl_\perp^2 d\tilde{t}}. \quad (8)$$

In this study, we take the higher-twist energy loss formalism [72,74,91,92] for the gluon emission spectrum off a heavy quark inside a dense nuclear medium,

$$\frac{dN_g^a}{dx\, dl_\perp^2 d\tilde{t}} = \frac{2C_A\alpha_{\rm s}P_a(x)l_\perp^4\hat{q}_a}{\pi\left(l_\perp^2+x^2m_a^2\right)^4}\sin^2\left(\frac{\tilde{t}-\tilde{t}_i}{2\tau_f}\right). \quad (9)$$

In the above two equations, E_a and m_a are the energy and mass of heavy quarks, x and $l_\perp$ represent the energy fraction and the transverse momentum of the radiated gluon with respect to the parent heavy quark, and $P_a(x)$ is the vacuum splitting function. The jet transport coefficient $\hat{q}_a$ represents the average transverse momentum squared exchanged between heavy quarks and the medium constituents per unit time during the elastic scattering process. Inside the sine function, $\tilde{t}-\tilde{t}_i$ is the time accumulated from the previous emission time ($\tilde{t}_i$), and $\tau_f = 2E_ax(1-x)/(l_\perp^2+x^2m_a^2)$ denotes the formation time of gluon emission. Based on the above formula, the probability for a heavy quark to experience inelastic scatterings with the QGP constituents during a time step $\Delta\tilde{t}$ can be calculated as $P_{\rm inel}^a = 1 - e^{-\Gamma_{\rm inel}^a\Delta\tilde{t}}$.

To include both elastic and inelastic scatterings between heavy quarks and the QGP medium, the total scattering rate can be obtained as $\Gamma_{\rm tot} = \Gamma_{\rm el} + \Gamma_{\rm inel}$. In terms of the total scattering probability, one may write out the following expression:

$$P_{\rm tot}^a = 1 - e^{-\Gamma_{\rm tot}\Delta t} = P_{\rm el}^a + P_{\rm inel}^a - P_{\rm el}^aP_{\rm inel}^a, \quad (10)$$

where $P_{\rm el}^a(1-P_{\rm inel}^a)$ can be understood as the pure elastic scattering probability, and $P_{\rm inel}^a$ is the inelastic scattering probability. Following our earlier work [20,59,86], we use different values of the coupling strength $\alpha_{\rm s}$ for different interaction vertices in our calculation of elastic and

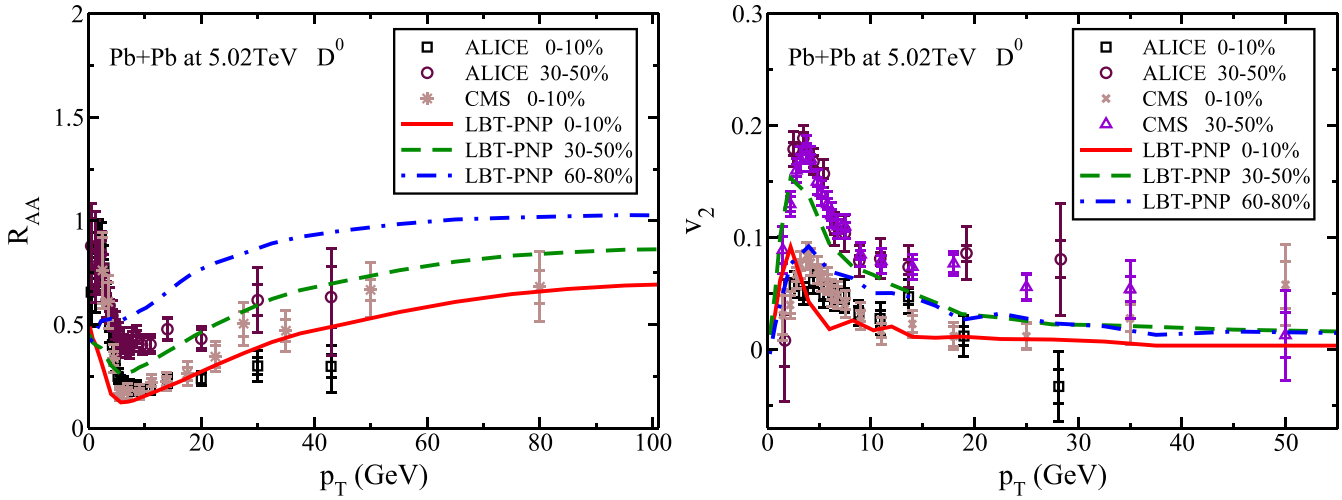

FIG. 1. R_{AA} and v_2 of the prompt D^0 mesons as functions of p_T in 0–10%, 30–50%, and 60–80% Pb+Pb collisions at $\sqrt{s_{NN}} = 5.02$ TeV, compared to the ALICE and CMS data for 0–10% and 30–50% centralities [23,68,103,104].

inelastic scatterings. For a vertex connecting to the propagating heavy quarks, we take $\alpha_s = 4\pi/[9\ln(2ET/\Lambda^2)]$ with $\Lambda = 0.2$ GeV; for a vertex connecting to the medium partons, we use the same value as in the interaction potential $V(r)$.

To evolve heavy quarks through a realistic medium, we utilize the (3+1)-dimensional viscous hydrodynamic model CLVISC [93–96] to simulate the dynamical evolution of the QGP fireball produced in relativistic heavy-ion collisions at the LHC. In the present study, we apply smooth hydrodynamic profiles for investigating heavy quarks, whose specific shear viscosity is taken to be $\eta/s = 0.16$ for the QGP produced in Pb+Pb collision at $\sqrt{s_{NN}} = 5.02$ TeV. The initial energy density distribution of the QGP is obtained from the Glauber model, which is also used to obtain the initial spatial distribution of heavy quarks. The momentum distribution of heavy quarks is initialized using the fixed-order next-to-leading-log (FONLL) calculation [97–99], where the parton distribution functions are taken from CT14NLO [100], and the nuclear shadowing effect is taken from EPPS16 [101] at the next-to-leading order. After their production, heavy quarks are assumed to stream freely before starting interaction with the QGP at the initial proper time of hydrodynamic evolution ($\tau_0 = 0.6$ fm/c). Interaction between heavy quarks and the QGP ceases when heavy quarks reach the QGP boundary, the hypersurface with $T_c = 165$ MeV in this work, on which they are converted into heavy flavor hadrons via a hybrid fragmentation-coalescence model [63]. In this hadronization model, the coalescence probability between heavy quarks and thermal light quarks are calculated according to the wave function overlap between the free-quark state and the hadronic bound state. Both s and p wave hadronic states are included, which naturally cover the majority of the observed heavy flavor hadron states. Based on this probability, heavy quarks that do not hadronize through coalescence are fragmented into heavy flavor hadrons via PYTHIA [102]. The decay of B mesons into nonprompt D^0 and J/ψ is also simulated by PYTHIA.

III. NUMERICAL RESULTS

In this section, we present our numerical results on the nuclear modification factor (R_{AA}) and elliptic flow coefficient (v_2) of nonprompt D^0 and J/ψ in Pb+Pb collisions at $\sqrt{s_{NN}} = 5.02$ TeV at the LHC.

Before showing results for nonprompt D^0 and J/ψ, we first show in Fig. 1 the R_{AA} and v_2 of prompt D^0 mesons as functions of transverse momentum p_T in Pb+Pb collisions at $\sqrt{s_{NN}} = 5.02$ TeV for three different centrality classes: central (0–10%), mid-central (30–50%), and peripheral (60–80%) collisions. The ALICE and CMS data on 0–10% and 30–50% centralities are shown for comparison. Our model can provide a reasonable description of the LHC data on the D^0 meson R_{AA} and v_2. One can see that both R_{AA} and v_2 show strong centrality dependence. From central to mid-central to peripheral collisions, the quenching of the prompt D mesons decreases (R_{AA} becomes larger) at large p_T due to the decreasing system size, whereas the prompt D meson v_2 first increases and then decreases due to the competition between the medium size and its geometric asymmetry. At high p_T, the heavy flavor v_2 originates from the asymmetric energy loss along different directions through the QGP. A smaller medium size at larger centrality causes weaker energy loss and weaker v_2 of heavy quarks; while an enhanced geometric asymmetry at larger centrality leads to larger heavy quark v_2. At low to medium p_T, the heavy flavor v_2 is also strongly affected by the anisotropic flow of the QGP background, which typically peaks at mid-centrality due to the competition between the medium size and its geometric asymmetry. As a result, the heavy flavor v_2 is expected to be strongest at mid-centrality. Meanwhile, both R_{AA} and v_2 show strong p_T dependence. The prompt D meson R_{AA} first exhibits a bump structure at low p_T and then increases with p_T at high p_T, whereas the prompt D meson v_2 first increases and then decreases. These structures originate from the combined effect of heavy quark spectrum, energy loss and hadronization, together with the QGP flow. At large p_T, the quenching of prompt D mesons mainly comes

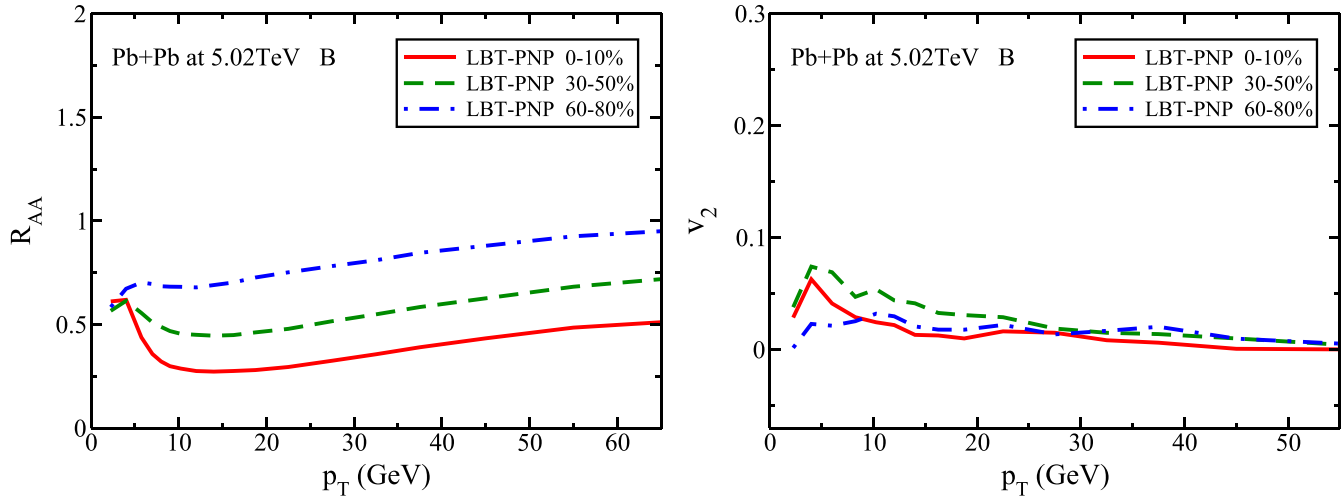

FIG. 2. R_{AA} and v_2 of B mesons as functions of p_T in 0–10%, 30–50%, and 60–80% Pb+Pb collisions at $\sqrt{s_{NN}} = 5.02$ TeV.

from charm quark energy loss inside the QGP, and the v_2 of prompt D mesons mainly results from the anisotropic energy loss along different directions through a geometrically asymmetric medium. The decreasing fractional energy loss and the flatter p_T spectrum of charm quarks at high p_T lead to the increasing R_{AA} and decreasing v_2 of prompt D mesons with p_T. At low to intermediate p_T, the strong nonperturbative interactions can quickly drive heavy quarks towards thermal equilibrium with the QGP, and therefore the motions of heavy quarks are strongly affected by the QGP flow. In addition, the coalescence between heavy quarks and the medium partons dominates the heavy flavor hadron formation at low to intermediate p_T, which further enhances the QGP flow effect on the prompt D meson spectrum. These lead to the flow bump of the prompt D meson R_{AA}, and the increasing D meson v_2 at low p_T, similar to the behaviors of light flavor hadron R_{AA} and v_2 observed at low p_T.

Figure 2 shows our prediction for the R_{AA} and v_2 of B mesons as functions of p_T in Pb+Pb collisions at $\sqrt{s_{NN}} =$ 5.02 TeV for 0–10%, 30–50%, and 60–80% centrality classes. Here, results for B mesons include contributions from B^+ and B^- in our simulation. Similar to previous results for prompt D mesons, the B meson R_{AA} and v_2 also show strong centrality dependence. Moving from central to mid-central to peripheral collisions, the quenching of B mesons becomes weaker due to the decreasing system size, while the B meson v_2 first increases and then decreases due to the combined effect of medium eccentricity and size. For the same centrality class, the B meson R_{AA} is larger than the prompt D meson R_{AA} at low p_T, while the former is comparable to the latter or even slightly smaller than the latter at high p_T. This is due to the nontrivial mass hierarchy of quark energy loss within our LBT-PNP model, as discussed in an earlier study [106]: b quarks lose less energy than c quarks at low p_T due to the "dead cone effect" in the gluon emission process, while the former may lose more energy than the latter at high p_T due to the string interaction implemented in our model. Within the same centrality class, the v_2 of B mesons is smaller than

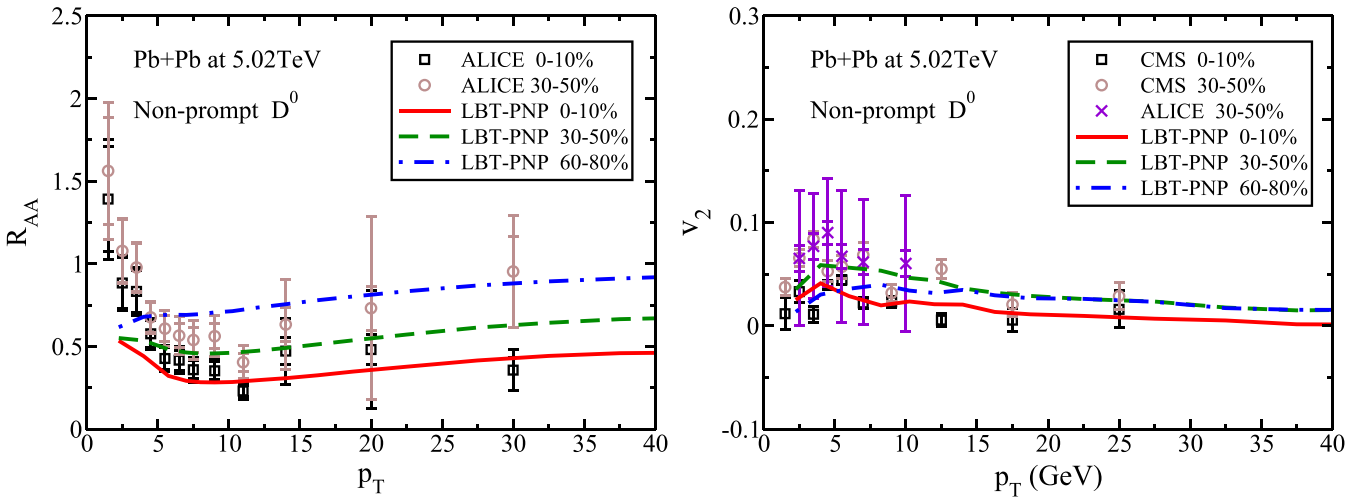

FIG. 3. R_{AA} and v_2 of nonprompt D^0 as functions of p_T in 0–10%, 30–50%, and 60–80% Pb+Pb collisions at $\sqrt{s_{NN}} = 5.02$ TeV, compared to the ALICE data for 0–10% and 30–50% centralities [76,77,105].

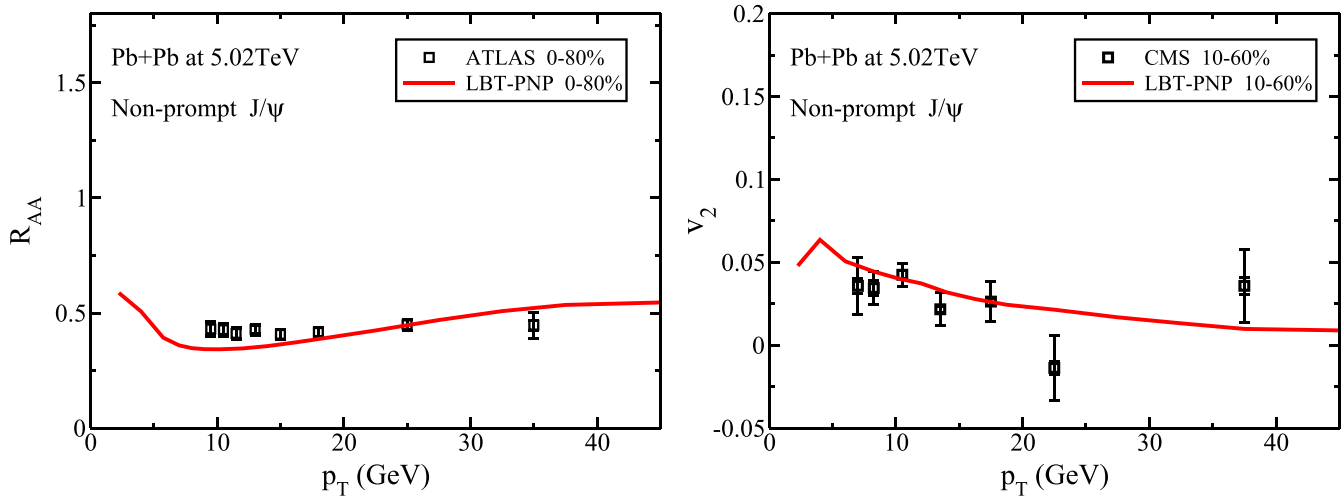

FIG. 4. R_{AA} (0–80% centrality) and v_2 (10–60% centrality) of nonprompt J/Ψ as functions of p_T in Pb+Pb collisions at $\sqrt{s_{NN}} = 5.02$ TeV, compared to the ATLAS and CMS data [79,83].

that of prompt D mesons at low p_T. At high p_T, they are both small.

To further study the quenching and flow of B mesons, Recently, ALICE, ATLAS and CMS Collaborations have measured the R_{AA} and v_2 of nonprompt D^0 and J/ψ, decayed from bottom hadrons [75–79,83,84]. In Fig. 3, we show the R_{AA} and v_2 for nonprompt D^0 from B meson decay as functions of p_T in central (0–10%), mid-central (30–50%) and peripheral (60–80%) Pb+Pb collisions at $\sqrt{s_{NN}} = 5.02$ TeV, compared to the ALICE and CMS data for 0–10% and 30–50% centralities. One can see that our model provides a reasonable description of the nonprompt D^0 meson R_{AA} and v_2 at high p_T. At low p_T, our model underestimates both R_{AA} and v_2, which may result from deficiencies in evaluating non-perturbative processes at low p_T, including the initial heavy quark spectra, string interactions between heavy quarks and the QGP, and hadronization of heavy quarks. Similar to prompt D and B mesons, the R_{AA} and v_2 of B-decayed D^0 mesons here also show strong dependence on centrality. In the same centrality class, the R_{AA} and v_2 of B-decayed D^0 show similar behaviors as those of B mesons, except for some p_T shift during the decay from B mesons to D mesons.

In Fig. 4, we show the R_{AA} of nonprompt J/ψ from B meson decay as a function of p_T in 0–80% Pb+Pb collisions at $\sqrt{s_{NN}} = 5.02$ TeV and the v_2 of nonprompt J/ψ from B meson decay in 10–60% collisions. Our model provides a good description of the corresponding ATLAS data on R_{AA} and the CMS data on v_2 of nonprompt J/ψ. Both the R_{AA} and v_2 results here are obtained from averaging over a large interval of centrality. They do not show a strong dependence on p_T.

In order to investigate the centrality dependence of quenching and flow of nonprompt J/ψ from B meson decay, we present in Fig. 5 the R_{AA} and v_2 of nonprompt J/ψ as func-

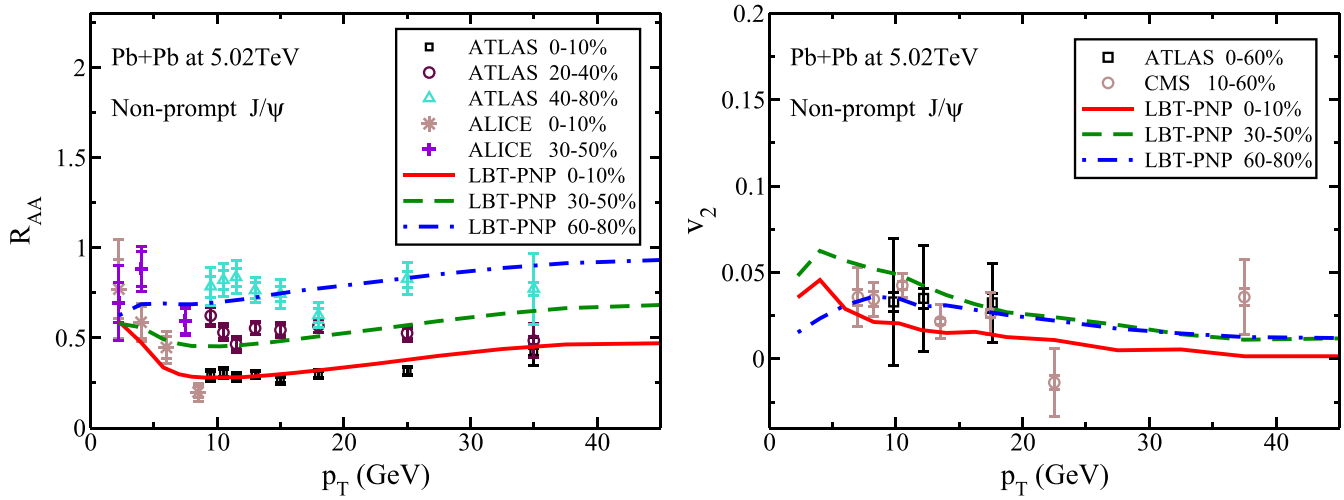

FIG. 5. R_{AA} and v_2 of nonprompt J/Ψ as functions of p_T in 0–10%, 30–50%, and 60–80% Pb+Pb collisions at $\sqrt{s_{NN}} = 5.02$ TeV, compared to the ALICE, ATLAS, and CMS data for various centralities [78,79,83,84].

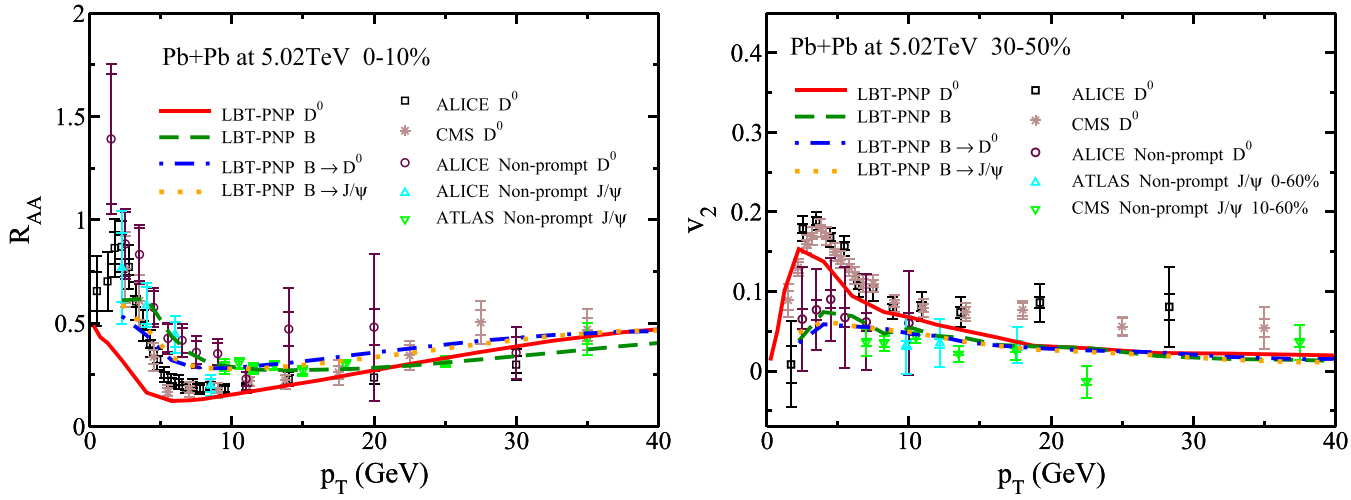

FIG. 6. R_{AA} (0–10% centrality) and v_2 (30–50% centrality) of prompt D^0, B, nonprompt D^0, and nonprompt J/Ψ as functions of p_T in Pb+Pb collisions at $\sqrt{s_{NN}} = 5.02$ TeV, compared to the available ALICE, ATLAS, and CMS data [23,68,76–79,83,84,103–105].

tions of p_T in central (0–10%), mid-central (30–50%) and peripheral (60–80%) Pb+Pb collisions at $\sqrt{s_{NN}} = 5.02$ TeV, compared to the available data from the ALICE, ATLAS, and CMS Collaborations. One can see that our model provides a reasonable description of the corresponding data within comparable centrality bins. Similar to previous results of prompt D mesons, B mesons and nonprompt D^0, the R_{AA} and v_2 of nonprompt J/ψ show strong centrality dependence.

In Fig. 6, we directly compare the quenching and flow between different species of heavy flavor particles presented above, left panel for the R_{AA} of prompt D, B, nonprompt D^0 and J/ψ from B meson decay in central (0–10%) Pb+Pb collisions at $\sqrt{s_{NN}} = 5.02$ TeV, and right panel for their v_2 in mid-central (30–50%) collisions, in comparison to the available ALICE, ATLAS, and CMS data. As discussed earlier, the R_{AA} of direct D mesons is smaller than that of B mesons at low p_T, while the inverse order is seen at high p_T. This is because of the opposite mass dependences of quark energy loss at low p_T and high p_T within our LBT-PNP model. In mid-central collisions, the v_2 of direct D mesons appear larger than that of B mesons. The R_{AA} of B-decayed D^0 and B-decayed J/ψ are smaller than that of B mesons at low p_T, but larger at high p_T, due to the p_T shift during the decay of B mesons. The v_2 of B-decayed D^0 and B-decayed J/ψ are smaller than that of B mesons at low p_T, but comparable at high p_T. No apparent difference in R_{AA} and v_2 is observed between B-decayed D^0 and B-decayed J/ψ due to their similar decay functions from B mesons.

In Fig. 7, we compare the p_T-integrated R_{AA} between prompt D^0, B, nonprompt D^0 and nonprompt J/ψ from B meson decay in Pb+Pb collisions at $\sqrt{s_{NN}} = 5.02$ TeV, left panel for $1.5 < p_T < 10$ GeV and right panel for $9 < p_T < 40$ GeV.

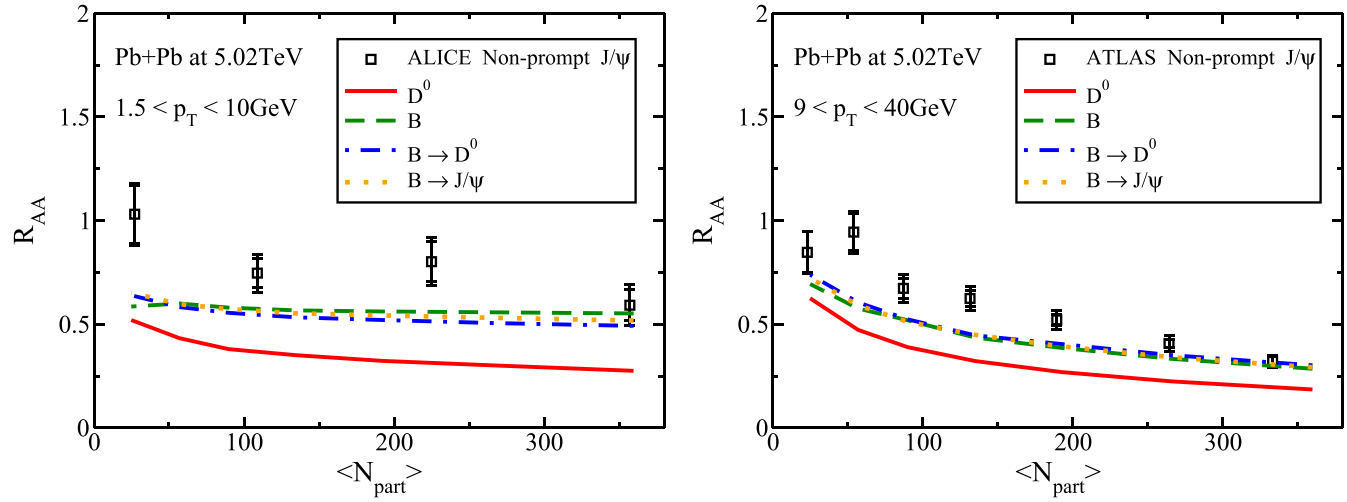

FIG. 7. R_{AA} of prompt D^0, B, nonprompt D^0, and nonprompt J/Ψ, integrated over $1.5 < p_T < 10$ GeV (left panel) and $9 < p_T < 40$ GeV (right panel), as functions of the participant nucleon number in Pb+Pb collisions at $\sqrt{s_{NN}} = 5.02$ TeV, compared to the available ALICE and ATLAS data [79,84].

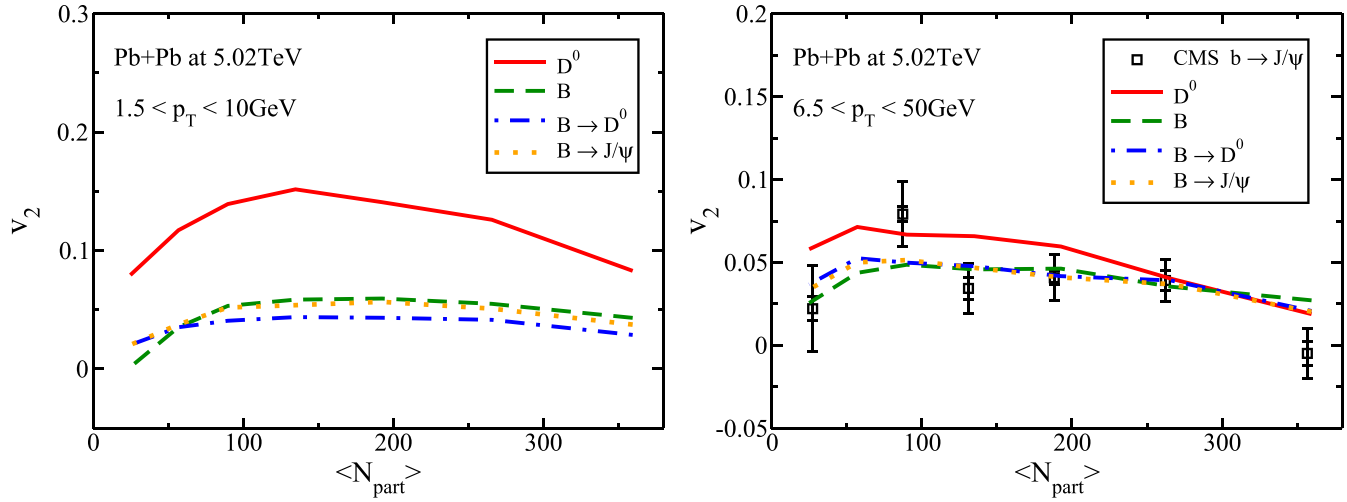

FIG. 8. v_2 of prompt D^0, B, nonprompt D^0, and nonprompt J/Ψ, integrated over $1.5 < p_T < 10$ GeV (left panel) and $6.5 < p_T < 50$ GeV (right panel), as functions of the participant nucleon number in Pb+Pb collisions at $\sqrt{s_{NN}} = 5.02$ TeV, compared to the available CMS data [83].

At higher p_T region (right panel), a clear participant number ($N_{\rm part}$), or centrality, dependence of R_{AA} can be seen for these heavy flavor particles: stronger energy loss of heavy quarks in more central collisions (larger $N_{\rm part}$) leads to smaller R_{AA}. This trend is not apparent at low p_T (left panel), where in addition to parton energy loss, the hadronization process and the QGP flow also significantly affect the final state hadron spectra. Within the p_T range we explore here, the R_{AA} of direct D mesons is smaller than that of B mesons. No obvious difference is observed between B mesons, B-decayed D^0 and B-decayed J/ψ in these p_T-integrated R_{AA}. Since our current model underestimates the heavy flavor R_{AA} at low p_T, as shown in previous p_T-dependent R_{AA} results, our result on the p_T-integrated R_{AA} of nonprompt J/ψ here is also lower than the available data from the ALICE and ATLAS Collaborations. The agreement becomes better as the p_T range becomes higher.

In the end, we compare in Fig. 8 the p_T-integrated v_2 between prompt D^0, B, nonprompt D^0, and nonprompt J/ψ from B meson decay in Pb+Pb collisions at $\sqrt{s_{NN}} = 5.02$ TeV, left panel for $1.5 < p_T < 10$ GeV and right panel for $6.5 < p_T < 50$ GeV. Moving from central to mid-central to peripheral collisions, or as $N_{\rm part}$ becomes smaller, the elliptic flow coefficients first increase and then decrease due to the combined effect of medium eccentricity and medium size. At low p_T, the prompt D^0 mesons have much larger v_2 than B mesons, nonprompt D^0 and nonprompt J/ψ. This difference becomes smaller at higher p_T. Compared to the available data from the CMS Collaboration, our model provides a reasonable description of the v_2 of nonprompt J/ψ.

IV. SUMMARY

Within the linear Boltzmann transport model that includes both string and Yukawa types of interactions between heavy quarks and the QGP, we study the dynamics of bottom quarks in Pb+Pb collisions at $\sqrt{s_{NN}} = 5.02$ TeV at the LHC via the nuclear modification factors and elliptic flow coefficients of B mesons, B-decayed D^0 and J/ψ. Compared to direct D mesons, B mesons show larger R_{AA} at low p_T but slightly smaller R_{AA} at high p_T, indicating weaker energy loss of heavier quarks at low p_T but a possible inverse order at high p_T within our LBT-PNP model. Both R_{AA} and v_2 of D and B mesons show strong p_T and centrality dependences. At high p_T, the heavy meson R_{AA} increases with p_T due to the decreasing fractional energy loss and the flatter p_T spectra of heavy quarks at higher p_T. A bump structure of R_{AA} can be observed at low p_T, resulting from the QGP flow effect and the coalescence process of heavy quark hadronization. The heavy meson v_2 is driven by the anisotropic QGP flow at low p_T, while driven by anisotropic energy loss through different directions at high p_T, and therefore, first increases and then decreases as p_T becomes larger. From central to mid-central to peripheral collisions, the heavy meson R_{AA} becomes larger due to weaker energy loss through a smaller QGP system. On the other hand, their v_2 first increases due to larger medium eccentricity, and then decreases due to smaller medium size. Nonprompt D^0 and nonprompt J/ψ from B meson decay show very similar R_{AA} and v_2 to B mesons, except for a shift towards the lower p_T region. Compared to the available ALICE, ATLAS and CMS data, our model provides a reasonable description of the nuclear modification factors and elliptic flow coefficients of prompt D mesons, nonprompt D^0 and nonprompt J/ψ, except for some deviation at low p_T due to possible inaccurate description of initial spectrum of heavy quarks, their interaction with the QGP and their hadronization process in this nonperturbative region. Therefore, studying nonprompt D^0 and J/ψ provides a supplementary way for better understanding heavy quark dynamics in relativistic heavy-ion collisions.

ACKNOWLEDGMENTS

This work is supported in part by the National Natural Science Foundation of China (NSFC) under Grants No.

12225503, No. 11890710, No. 11890711, No. 11935007, No. 12175122, and No. 2021-867. W.-J.X. is supported in part by China Postdoctoral Science Foundation under Grant No. 2023M742099. Some of the calculations were performed in the Nuclear Science Computing Center at Central China Normal University (NSC^3), Wuhan, Hubei, China.

[1] M. Gyulassy and L. McLerran, Nucl. Phys. A **750**, 30 (2005).
[2] B. Müller, J. Schukraft, and B. Wyslouch, Annu. Rev. Nucl. Part. Sci. **62**, 361 (2012).
[3] P. Romatschke and U. Romatschke, *Relativistic Fluid Dynamics In and Out of Equilibrium*, Cambridge Monographs on Mathematical Physics (Cambridge University Press, Cambridge, 2019).
[4] D. H. Rischke, S. Bernard, and J. A. Maruhn, Nucl. Phys. A **595**, 346 (1995).
[5] U. Heinz and R. Snellings, Annu. Rev. Nucl. Part. Sci. **63**, 123 (2013).
[6] C. Gale, S. Jeon, and B. Schenke, Int. J. Mod. Phys. A **28**, 1340011 (2013).
[7] P. Huovinen, Int. J. Mod. Phys. E **22**, 1330029 (2013).
[8] X.-N. Wang and M. Gyulassy, Phys. Rev. Lett. **68**, 1480 (1992).
[9] M. Gyulassy, I. Vitev, X.-N. Wang, and B.-W. Zhang, in *Quark Gluon Plasma 3*, edited by R. C. Hwa and X.-N. Wang (World Scientific, Singapore, 2004), pp. 123–191.
[10] A. Majumder and M. Van Leeuwen, Prog. Part. Nucl. Phys. **66**, 41 (2011).
[11] G.-Y. Qin and X.-N. Wang, Int. J. Mod. Phys. E **24**, 1530014 (2015).
[12] J.-P. Blaizot and Y. Mehtar-Tani, Int. J. Mod. Phys. E **24**, 1530012 (2015).
[13] S. Cao and X.-N. Wang, Rep. Prog. Phys. **84**, 024301 (2021).
[14] S. Cao and G.-Y. Qin, Annu. Rev. Nucl. Part. Sci. **73**, 205 (2023).
[15] X. Dong, Y.-J. Lee, and R. Rapp, Annu. Rev. Nucl. Part. Sci. **69**, 417 (2019).
[16] A. Andronic *et al.*, Eur. Phys. J. C **76**, 107 (2016).
[17] M. He, H. van Hees, and R. Rapp, Prog. Part. Nucl. Phys. **130**, 104020 (2023).
[18] S. Cao, G.-Y. Qin, and S. A. Bass, Phys. Rev. C **88**, 044907 (2013).
[19] S. Cao, T. Luo, G.-Y. Qin, and X.-N. Wang, Phys. Rev. C **94**, 014909 (2016).
[20] W.-J. Xing, S. Cao, G.-Y. Qin, and H. Xing, Phys. Lett. B **805**, 135424 (2020).
[21] F.-L. Liu *et al.*, Eur. Phys. J. C **82**, 350 (2022).
[22] L. Adamczyk *et al.* (STAR Collaboration), Phys. Rev. Lett. **113**, 142301 (2014); **121**, 229901(E) (2018).
[23] A. M. Sirunyan *et al.* (CMS Collaboration), Phys. Lett. B **782**, 474 (2018).
[24] J. Adam *et al.* (STAR Collaboration), Phys. Rev. C **99**, 034908 (2019).
[25] P. B. Gossiaux, V. Guiho, and J. Aichelin, J. Phys. G **32**, S359 (2006).
[26] G.-Y. Qin and A. Majumder, Phys. Rev. Lett. **105**, 262301 (2010).
[27] J. Uphoff, O. Fochler, Z. Xu, and C. Greiner, Phys. Rev. C **84**, 024908 (2011).
[28] C. Young, B. Schenke, S. Jeon, and C. Gale, Phys. Rev. C **86**, 034905 (2012).
[29] W. Alberico *et al.*, Eur. Phys. J. C **71**, 1666 (2011).
[30] O. Fochler, J. Uphoff, Z. Xu, and C. Greiner, Phys. Rev. D **88**, 014018 (2013).
[31] M. Nahrgang, J. Aichelin, P. B. Gossiaux, and K. Werner, Phys. Rev. C **90**, 024907 (2014).
[32] M. Djordjevic and M. Djordjevic, Phys. Lett. B **734**, 286 (2014).
[33] S. Cao, G.-Y. Qin, and S. A. Bass, Phys. Rev. C **92**, 024907 (2015).
[34] S. K. Das, F. Scardina, S. Plumari, and V. Greco, Phys. Lett. B **747**, 260 (2015).
[35] T. Song, H. Berrehrah, D. Cabrera, W. Cassing, and E. Bratkovskaya, Phys. Rev. C **93**, 034906 (2016).
[36] Z.-B. Kang, F. Ringer, and I. Vitev, J. High Energy Phys. 03 (2017) 146.
[37] C. A. G. Prado, J. Noronha-Hostler, R. Katz, A. A. P. Suaide, J. Noronha, and M. G. Munhoz, Phys. Rev. C **96**, 064903 (2017).
[38] Y. Xu, J. E. Bernhard, S. A. Bass, M. Nahrgang, and S. Cao, Phys. Rev. C **97**, 014907 (2018).
[39] S. Y. F. Liu and R. Rapp, Phys. Rev. C **97**, 034918 (2018).
[40] A. Beraudo *et al.*, Nucl. Phys. A **979**, 21 (2018).
[41] S. Cao *et al.*, Phys. Rev. C **99**, 054907 (2019).
[42] S. Li, C. Wang, X. Yuan, and S. Feng, Phys. Rev. C **98**, 014909 (2018).
[43] W. Ke, Y. Xu, and S. A. Bass, Phys. Rev. C **98**, 064901 (2018).
[44] S. Li, C. Wang, R. Wan, and J. Liao, Phys. Rev. C **99**, 054909 (2019).
[45] R. Katz, C. A. Prado, J. Noronha-Hostler, J. Noronha, and A. A. Suaide, Phys. Rev. C **102**, 024906 (2020).
[46] S.-Q. Li, W.-J. Xing, F.-L. Liu, S. Cao, and G.-Y. Qin, Chin. Phys. C **44**, 114101 (2020).
[47] B. Chen, L. Wen, and Y. Liu, Phys. Lett. B **834**, 137448 (2022).
[48] M. Yang, S. Zheng, B. Tong, J. Zhao, W. Ouyang, K. Zhou, and B. Chen, Phys. Rev. C **107**, 054917 (2023).
[49] F.-L. Liu, X.-Y. Wu, S. Cao, G.-Y. Qin, and X.-N. Wang, Phys. Lett. B **848**, 138355 (2024).
[50] J.-Y. Ollitrault, Phys. Rev. D **46**, 229 (1992).
[51] K. H. Ackermann *et al.* (STAR Collaboration), Phys. Rev. Lett. **86**, 402 (2001).
[52] C. Adler *et al.* (STAR Collaboration), Phys. Rev. Lett. **87**, 182301 (2001).
[53] K. Aamodt *et al.* (ALICE Collaboration), Phys. Rev. Lett. **105**, 252302 (2010).
[54] K. Aamodt *et al.* (ALICE Collaboration), Phys. Rev. Lett. **107**, 032301 (2011).
[55] B. Alver and G. Roland, Phys. Rev. C **81**, 054905 (2010).
[56] G.-Y. Qin, H. Petersen, S. A. Bass, and B. Muller, Phys. Rev. C **82**, 064903 (2010).
[57] G. D. Moore and D. Teaney, Phys. Rev. C **71**, 064904 (2005).
[58] M. He, R. J. Fries, and R. Rapp, Phys. Rev. C **86**, 014903 (2012).

[59] W.-J. Xing, G.-Y. Qin, and S. Cao, Phys. Lett. B **838**, 137733 (2023).
[60] S. Plumari, V. Minissale, S. K. Das, G. Coci, and V. Greco, Eur. Phys. J. C **78**, 348 (2018).
[61] M. He and R. Rapp, Phys. Rev. Lett. **124**, 042301 (2020).
[62] S. Cho, K.-J. Sun, C. M. Ko, S. H. Lee, and Y. Oh, Phys. Rev. C **101**, 024909 (2020).
[63] S. Cao *et al.*, Phys. Lett. B **807**, 135561 (2020).
[64] J. Zhao *et al.*, Phys. Rev. C **109**, 054912 (2024).
[65] L. Adamczyk *et al.* (STAR Collaboration), Phys. Rev. Lett. **118**, 212301 (2017).
[66] A. M. Sirunyan *et al.* (CMS Collaboration), Phys. Rev. Lett. **120**, 202301 (2018).
[67] S. Acharya *et al.* (ALICE Collaboration), Phys. Rev. Lett. **120**, 102301 (2018).
[68] S. Acharya *et al.* (ALICE Collaboration), Phys. Lett. B **813**, 136054 (2021).
[69] A. Kusina, J.-P. Lansberg, I. Schienbein, and H.-S. Shao, Phys. Rev. Lett. **121**, 052004 (2018).
[70] Y. L. Dokshitzer and D. E. Kharzeev, Phys. Lett. B **519**, 199 (2001).
[71] N. Armesto, C. A. Salgado, and U. A. Wiedemann, Phys. Rev. D **69**, 114003 (2004).
[72] B.-W. Zhang, E. Wang, and X.-N. Wang, Phys. Rev. Lett. **93**, 072301 (2004).
[73] M. Djordjevic and M. Gyulassy, Nucl. Phys. A **733**, 265 (2004).
[74] L. Zhang, D.-F. Hou, and G.-Y. Qin, Phys. Rev. C **100**, 034907 (2019).
[75] A. M. Sirunyan *et al.* (CMS Collaboration), Phys. Rev. Lett. **123**, 022001 (2019).
[76] S. Acharya *et al.* (ALICE Collaboration), J. High Energy Phys. 12 (2022) 126.
[77] S. Acharya *et al.* (ALICE Collaboration), Eur. Phys. J. C **83**, 1123 (2023).
[78] M. Aaboud *et al.* (ATLAS Collaboration), Eur. Phys. J. C **78**, 784 (2018).
[79] M. Aaboud *et al.* (ATLAS Collaboration), Eur. Phys. J. C **78**, 762 (2018).
[80] G. Aad *et al.* (ATLAS Collaboration), Phys. Lett. B **807**, 135595 (2020).
[81] G. Aad *et al.* (ATLAS Collaboration), Phys. Lett. B **829**, 137077 (2022).
[82] S. Acharya *et al.* (ALICE Collaboration), Phys. Lett. B **804**, 135377 (2020).
[83] A. Tumasyan *et al.* (CMS Collaboration), J. High Energy Phys. 10 (2023) 115.
[84] S. Acharya *et al.* (ALICE Collaboration), J. High Energy Phys. 01 (2024) 147.
[85] Y. He, T. Luo, X.-N. Wang, and Y. Zhu, Phys. Rev. C **91**, 054908 (2015).
[86] S. Cao, T. Luo, G.-Y. Qin, and X.-N. Wang, Phys. Lett. B **777**, 255 (2018).
[87] B. Combridge, Nucl. Phys. B **151**, 429 (1979).
[88] B. Svetitsky, Phys. Rev. D **37**, 2484 (1988).
[89] M. G. Mustafa, D. Pal, and D. K. Srivastava, Phys. Rev. C **57**, 889 (1998).
[90] S. Y. F. Liu and R. Rapp, Eur. Phys. J. A **56**, 44 (2020).
[91] X.-F. Guo and X.-N. Wang, Phys. Rev. Lett. **85**, 3591 (2000).
[92] A. Majumder, Phys. Rev. D **85**, 014023 (2012).
[93] L. Pang, Q. Wang, and X.-N. Wang, Phys. Rev. C **86**, 024911 (2012).
[94] L.-G. Pang, H. Petersen, and X.-N. Wang, Phys. Rev. C **97**, 064918 (2018).
[95] X.-Y. Wu, L.-G. Pang, G.-Y. Qin, and X.-N. Wang, Phys. Rev. C **98**, 024913 (2018).
[96] X.-Y. Wu, G.-Y. Qin, L.-G. Pang, and X.-N. Wang, Phys. Rev. C **105**, 034909 (2022).
[97] M. Cacciari, S. Frixione, and P. Nason, J. High Energy Phys. 03 (2001) 006.
[98] M. Cacciari *et al.*, J. High Energy Phys. 10 (2012) 137.
[99] M. Cacciari, M. L. Mangano, and P. Nason, Eur. Phys. J. C **75**, 610 (2015).
[100] S. Dulat *et al.*, Phys. Rev. D **93**, 033006 (2016).
[101] K. J. Eskola, P. Paakkinen, H. Paukkunen, and C. A. Salgado, Eur. Phys. J. C **77**, 163 (2017).
[102] T. Sjöstrand, S. Mrenna, and P. Z. Skands, J. High Energy Phys. 05 (2006) 026.
[103] S. Acharya *et al.* (ALICE Collaboration), J. High Energy Phys. 01 (2022) 174.
[104] A. M. Sirunyan *et al.* (CMS Collaboration), Phys. Lett. B **816**, 136253 (2021).
[105] A. Tumasyan *et al.* (CMS Collaboration), Phys. Lett. B **850**, 138389 (2024).
[106] Y. Dang, W.-J. Xing, S. Cao, and G.-Y. Qin, Phys. Rev. C **109**, 064901 (2024).